Translational Stroke Research (2020) 11:503–516
https://doi.org/10.1007/s12975-019-00739-2

ORIGINAL ARTICLE

# Quantitative Iron Neuroimaging Can Be Used to Assess the Effects of Minocycline in an Intracerebral Hemorrhage Minipig Model

Yang Yang[1] · Kaiyuan Zhang[1] · Xuntao Yin[2] · Xuejiao Lei[1] · Xuezhu Chen[1] · Ju Wang[1] · Yulian Quan[1] · Ling Yang[1] · Zhengcai Jia[1] · Qianwei Chen[1] · Jishu Xian[1] · Yongling Lu[3] · Qianying Huang[3] · Xuan Zhang[4] · Hua Feng[1] · Tunan Chen[1]

Received: 26 July 2019 / Revised: 9 September 2019 / Accepted: 10 September 2019 / Published online: 6 November 2019


## Abstract

Iron-mediated toxicity is a key factor causing brain injury after intracerebral hemorrhage (ICH). This study was performed to investigate the noninvasive neuroimaging method for quantifying brain iron content using a minipig ICH model and assess the effects of minocycline treatment on ICH-induced iron overload and brain injury. The minipig ICH model was established by injecting 2 ml of autologous blood into the right basal ganglia, which were then subjected to the treatments of minocycline and vehicle. Furthermore, the quantitative susceptibility mapping (QSM) was used to quantify iron content, and diffusion tensor imaging (DTI) was performed to evaluate white matter tract. Additionally, we also performed immunohistochemistry, Western blot, iron assay, Perl's staining, brain water content, and neurological score to evaluate the iron overload and brain injury. Interestingly, we found that the ICH-induced iron overload could be accurately quantified by the QSM. Moreover, the minocycline was quite beneficial for protecting brain injury by reducing the lesion volume and brain edema, preventing brain iron accumulation, downsizing ventricle enlargement, and alleviating white matter injury and neurological deficits. In summary, we suggest that the QSM be an accurate and noninvasive method for quantifying brain iron level, and the minocycline may be a promising therapeutic agent for patients with ICH.

**Keywords** Intracerebral hemorrhage · Minipig · Minocycline · Quantitative susceptibility mapping · Diffusion tensor imaging

## Introduction

Spontaneous intracerebral hemorrhage (ICH) is a life-threatening condition with poor prognosis, accounting for ~ 10–15% of stroke-related hospitalizations [1]. As an important degradation product of hemoglobin, brain iron overload serves essential roles in post-ICH brain injury [2]. Previous studies revealed that iron accumulation could last for several months following ICH [3], consequently resulting in hydrocephalus [4], neuronal death, white matter tract injury, and

Yang Yang and Kaiyuan Zhang contributed equally to this work.

**Electronic supplementary material** The online version of this article (https://doi.org/10.1007/s12975-019-00739-2) contains supplementary material, which is available to authorized users.

✉ Xuan Zhang
2721053836@qq.com

✉ Hua Feng
fenghua8888@vip.163.com

✉ Tunan Chen
ctn@tmmu.edu.cn

[1] Department of Neurosurgery and Key Laboratory of Neurotrauma, Southwest Hospital, The Third Military Medical University (Army Military Medical University), Chongqing, China

[2] Department of Radiology, Southwest Hospital, The Third Military Medical University (Army Military Medical University), Chongqing, China

[3] Clinical Research Center, The Third Military Medical University (Army Military Medical University), Chongqing, China

[4] Department of Neurosurgery, No. 989 Hospital of Joint Logistic Force (the 150th central hospital) of PLA, Luoyang, Henan Province, China

neurological deficit [5–7]. Furthermore, iron chelator-deferoxamine can alleviate ICH-induced brain injury in experimental and clinical researches [7, 8], suggesting that prevention of iron-mediated brain injury could be a promising therapeutic strategy for ICH. Thus, noninvasive and accurate method for quantification of iron content in hematoma was helpful for understanding of iron-mediated damage and assessing the prognosis after ICH in humans.

Recent study revealed that magnetic resonance imaging (MRI) R2* mapping was a quantitative method to evaluate post-ICH brain iron overload [9] and hepatic iron overload [10, 11]; however, MRI R2* mapping could not be used to determine the iron levels in hematoma at acute phase (too high) or in the cavity at chronic phase following ICH [12]. Susceptibility-weighted imaging and quantitative susceptibility mapping (SWI-QSM) has been recently introduced as a novel MRI post-processing technique of gradient-recalled echo (GRE) [13]. The QSM is more accurate and powerful for visualization of acute hemorrhage and determination of brain iron concentration compared with computed tomography (CT) and R2* mapping [14–16]. However, the roles of the QSM in the diagnosis and management of stroke have not been extensively investigated so far [17].

Minocycline is an inhibitor of microglial activation and iron chelator. Previous studies have revealed that minocycline is able to prevent ICH-induced brain iron overload and brain injury in rodent animals, and its efficacy is higher than deferoxamine [9, 18–20]. However, the effects of minocycline on patients with ICH have not been investigated in large prospective randomized trials yet [21]. Thus, preclinical pig ICH model could be established and used to determine the dosage, duration, and administration method of minocycline.

To evaluate the perihematomal iron using the SWI-QSM method, a minipig ICH model was established in the present study. Then, the model and neuroimaging methods were used to investigate whether minocycline could reduce the risk of ICH-induced iron overload, brain edema, and white matter injury.

## Materials and Methods

### Animal Experiments and Establishment of ICH Model

Male minipigs weighing ~ 10–12 kg were obtained from the Experimental Animal Center at the Third Military Medical University (permit no. Yu2017-0002; Chongqing, China) and used in the present study. All experiments are reported in compliance with the Animal Research: Reporting in Vivo Experiments (ARRIVE) guidelines. The experimental protocols were approved by the Ethics Committee of the Third Military Medical University and performed according to the guide for the care and use of laboratory animals. Randomization was carried out using odd/even numbers.

Minipigs were anesthetized using ketamine/xylazine (20/2.2 mg/kg, I.M.) and then inhaled with 3.0% isoflurane delivered via an esthetic mask. The concentration of isoflurane was ~ 1.0% during the surgery. The core temperature was maintained at 37.5 ± 0.5 °C using a thermostatic operation table (Golden Brains Optical Instrument Co., Ltd., Hefei, China). The right femoral artery was inserted with a polyethylene catheter (PE-160) to monitor arterial blood pressure and allow autologous blood injection. Then, the surgical procedure of ICH was performed using the aseptic techniques as previously described [5, 7] with minor modifications. A cranial burr hole (1 mm) was created at a specific site (bregma coordinates: 11 mm anterior and 11 mm lateral from the midline) by the guidance of digital stereotactic equipment. A sterile 33G needle (19 mm in length) with a syringe was placed stereotaxically into the center of the right cerebral white matter region at the level of the caudate nucleus. Then, 2 ml of autologous arterial blood was infused for 20 min using a microinfusion pump (Harvard Apparatus, Holliston, MA). Sham-operated minipigs underwent the same surgery without blood injection.

A total of 75 male minipigs were used in the present study, and the minipigs were randomly divided into 3 sections (Figure I in the supplementary information). In the first section, eight ICH pigs were deeply anesthetized at days 0, 1, 7, or 28 for MRI sequences scanning and analysis (T2*, SWI, and DTI). In the second section, ICH pigs were sacrificed at days 1 and 7 ($n = 5$–6/time point) and the controls were sacrificed at day 7 for brain water content, HE and Perls' staining, Western blotting, transmission electron microscopy, and immunohistochemistry analysis. In the third section, ICH minipigs were randomly treated with vehicle alone or minocycline (Sigma–Aldrich; 6 mg/kg I.P. at 2 h post-ICH followed by a maintenance dose of 3 mg/kg every 12 h for up to 7 days). At day 7 or 28, minipigs (5–6 pigs/time point in each group) were sacrificed after MRI, and then, the brains were harvested for morphology and molecular biology researches. Six pigs died from this study (mortality rate = 8.6%), two died during anesthesia, and four died in the ICH group. What is more, five pigs were excluded because of the incorrect location of hematoma.

### Magnetic Resonance Imaging and Analysis

MRI data were acquired using a 3.0-T MR scanner (Trio, Siemens Medical, Erlangen, Germany) and a 12-channel head coil. T2-weighted images were obtained with the following parameters: TR/TE = 200/2.78 ms, flip angle = 70°, matrix = 384 × 384, thickness = 2.4 mm, field of view = 230 × 230 $mm^2$, and voxel size = 0.5 × 0.5 × 2.4 mm3. What is more, the volume of ipsilateral and contralateral ventricles was measured by combining the total areas and multiplying by the thickness (2.4 mm) using an image analysis system (ImageJ). The volume of ipsilateral and contralateral ventricles at day 0 was expressed as 100%;

the enlargement of ipsilateral and contralateral ventricles at days 1, 7, and 28 after ICH or treatment was expressed as a percentage of day 0, respectively [9].

SWI was obtained using a high-resolution three-dimensional spoiled gradient-echo sequence with the following parameters: TR/TE = 29/20 ms, flip angle = 15°, section thickness = 2 mm, field of view = 256 × 256 $mm^2$, matrix size = 512 × 512, and voxel size = 0.5 × 0.5 × 2 $mm^3$. Susceptibility Mapping and Phase Artifacts Removal Toolbox (SMART; Detroit, MI, USA) and signal processing in nuclear magnetic resonance software (SPIN; MR Innovations Inc., Detroit, MI, USA) were used for the QSM processing and measurement [22–24]. To reconstruct the QSM of hematoma with minimal artifacts, the following steps were carried out according to detailed method in previous study [24]: (1) collect an isotropic high-resolution SWI dataset; (2) high-pass filter the phase images; (3) interpolate k-space; (4) remove spurious phase noise sources from the phase images; and (5) apply the regularized inverse filter to this data. Finally, a 0.1 threshold regularized inverse filter was applied. Regions of interest (ROI) were manually defined on each slice of the hematoma; then, the QSM of hematoma could be obtained. In addition, the volume of hematoma was measured by combining the total areas and multiplying by the thickness (2 mm) using ImageJ.

The parameters of diffusion tensor imaging (DTI) were set as follows: repetition time = 6000 ms, echo time = 89 ms, flip angle = 120°, field of view = 230 × 230 $mm^2$, slices = 84, thickness = 2.0 mm, matrix = 448 × 448, and voxel size = 0.5 × 0.5 × 2 $mm^3$. DTI was measured using a single-shot echo-planar sequence with the following parameters: slice number = 45, matrix = 128 × 128, slice thickness = 2 mm, TR = 6100 ms, and TE = 93 ms. Following an acquisition without diffusion, images were then acquired using diffusion gradients ($b$ = 1000 s/$mm^2$) applied in 64 directions (segments = 4; bandwidth = 2 × 106 Hz; $\beta$ value = 0, 1000 s/$mm^2$, repetition time/echo time = 3000/25 ms, thickness/gap = 1/0 mm, field of view = 30 × 30 mm, matrix = 128 × 128, and number of excitations = 4). Three-dimensional reconstructions were created to analyze white matter tracts using the Diffusion Toolkit software (Harvard Medical School, Boston) as previously described [25, 26]. Brain tissues adjacent to the hemorrhagic region were scanned using MRI-View3D software (ShockWatch, Graham, TX). The values of fractional anisotropy (FA) and apparent diffusion coefficient (ADC) were determined. FA was calculated using the three diagonal elements of the diagonalized diffusion tensor in ROI.

## Immunohistochemistry and Enhanced Perls' Staining

At day 28 after ICH, the brain tissues around hematoma of each group were dissected and fixed in 4% paraformaldehyde (PFA) for 24 h at 4 °C. Then, tissues were processed for paraffin embedding, and sections (5 μm thick) were collected for immunohistochemistry, hematoxylin–eosin (HE), and enhanced Perls' staining according to Yang et al. [27, 28]. For immunohistochemistry, after blocking of endogenous peroxidase activity, increasing permeability and blocking, sections were exposed to rabbit anti-ferritin monoclonal antibody (1:200; Abcam) in 1% BSA (12 h, 4 °C). Sections were then incubated with the avidin–biotin complex (1:200; DAKO), followed by the biotinylated secondary antibody (1:200; 2 h, 37 °C; DAKO), and finally, staining was visualized using the 3,3′-diaminobenzidine substrate kit (Vector Laboratories) and counterstained by hematoxylin. For enhanced Pelrs' staining, brain sections were incubated in Perls' solution (1:1, 5% potassium ferrocyanide and 5% HCl) for 45 min, washed in distilled water, and incubated again in 0.5% diamine benzidine tetrahydrochloride with nickel for 60 min. All the morphological results were photographed (× 20 magnification) using a Zeiss Axiovert microscope equipped with a digital color camera, and the positive cells in per square millimeter were counted and analyzed for comparison of each group in a double-blind manner.

## Transmission Electron Microscopy

Animals were sacrificed and perfused with PBS followed by fixation solution of 2.5% glutaraldehyde/2% paraformaldehyde in 0.1 M sodium cacodylate buffer (pH 7.4). Small pieces (1-$mm^3$ cubes) around hematoma from a perfusion-fixed animal were post-fixed for at least 2 h at RT in the above fixative, washed in 0.1 M cacodylate buffer and post-fixed with 1% osmium tetroxide (OsO4)/1.5% potassium ferrocyanide (KFeCN6) for 1 h, washed in water 3× and incubated in 1% aqueous uranyl acetate for 1 h, followed by 2 washes in water and subsequent dehydration in grades of alcohol (10 min each; 50%, 70%, 90%, 2 × 10 min 100%). The samples were then put in propylene oxide for 1 h and infiltrated ON in a 1:1 mixture of propylene oxide and TAAB Epon (Marivac Canada Inc., St. Laurent, Canada). In the following day, the samples were embedded in TAAB Epon and polymerized at 60 °C for 48 h. Ultrathin sections (60 nm) were cut with a ultramicrotome (LKB-V, LKB Produkter AB, Bromma, Sweden), picked up on to copper grids stained with lead citrate, and examined in a transmission electron microscope (TECNAI10, Philips, Eindhoven, The Netherlands), and images were recorded with an AMT 2k CCD camera. Myelination, axonal morphology, and g-ratios of different genotypes were determined from counting of 300~400 axons in the white matter of 4 pigs of each group using the ImageJ analysis.

## Neurological Examination

The neurological function was evaluated according to previous study with some modifications [29] and run blinded to the

experimental condition. Total neurological deficit included scores generated from a 25-point scale that assessed appetite (4 points), standing position (5), head position (2), utterance (2), gait (3), forelimb function(4), hindlimb function(4), and facial paresis (1) at days 1, 7, and 28 after ICH.

### Statistical Analysis

All the data collected in a double-blind manner and statistical analyses were performed using SPSS 18.0 software. Data were presented as mean ± SD and analyzed using a Student *t* test or analysis of variance (ANOVA). A Bonferroni test was used as a post hoc test following ANOVA. $P < 0.05$ was considered to indicate a statistically significant difference.

## Results

### Establishment of ICH Model in Minipigs

To generate an ICH model in minipigs, digital stereotaxic instrument, anesthetic machine, microinfusion pump, and 33G needles were used during surgery (Fig. 1a). In the established model, T2-weighted pictures were scanned for examining brain ventricle volume after ICH (Fig. 1b). Ipsilateral brain water content (%) was significantly increased at days 1 (85 ± 1.8 vs 73 ± 0.6%; $P < 0.01$) and 7 (82.4 ± 1.5 vs 73 ± 0.6%; $P < 0.01$) post-ICH, but returned to normal level at day 28 (74.2 ± 1 vs 73 ± 0.6%; $P > 0.05$) compared with the Sham group. However, contralateral brain water content (%) was increased at day 1 (76.2 ± 1.1 vs 72.8 ± 0.5%; $P < 0.05$), but there was no notable difference in between the ICH and Sham groups (Fig. 1c) at days 7 (73.8 ± 0.8%) and 28 (73.4 ± 0.5% vs 72.8 ± 0.5%, $P > 0.05$). The percentage of post-ICH lateral ventricle enlargement was determined using MRI-T2 (Fig. 1b). The ipsilateral ventricle shrank a little at day 1 (84.5 ± 5.7 vs 100%; $P > 0.05$) post-ICH compared with that prior to ICH due to the squeezing of hematoma and then significantly enlarged at day 7 (123.3 ± 14.2 vs 100%; $P < 0.05$) and 28 (177.9 ± 18.5 vs 100%; $P < 0.01$). Furthermore, the size of contralateral ventricle was remarkably increased at days 1 (162.1 ± 8.9 vs 100%; $P < 0.01$) and 7 (137.4 ± 12.8 vs 100%; $P < 0.05$) post-ICH and became normal at day 28 (127.7 ± 17.6 vs 100%; $P > 0.05$; Fig. 1d).

### SWI-QSM Accurately and Noninvasively Reflects Iron Deposition After ICH

SWI was performed to determine the volume of post-ICH lesion (Fig. 2a). The lesion volume of hematoma ($mm^3$) gradually decreased from day 1 to 28 (1 day, 2060 ± 204; 7 days, 1562 ± 314; 28 days, 1006 ± 174; Fig. 2b). However, the hematomal average susceptibility (ppb × $10^{-9}$; Pre, 28.4 ± 6.4; 1 day, 243.6 ± 28.2; 7 days, 220.1 ± 70.7; 28 days, 208.7 ± 13.6; Fig. 2a, c) and perihematomal iron content (μg/g; Sham, 3.4 ± 1.2; 1 day, 15 ± 2.9; 7 days, 13.1 ± 1.7; 28 days, 11.8 ± 2.8; Fig. 2d) had no significant reduction from day 1 to 28. Interestingly, the average susceptibility and iron content were positively correlated from day 1 to 28 ($R^2 = 0.93$; Fig. 2d).

### ICH-Induced Iron Overload and Overexpression of Iron-Handling Proteins in Perihematomal Region

Locally accumulated iron could be converted to hemosiderin by macrophages. The number of hemosiderin-positive cells was significantly increased at days 7 (348.5 ± 40.6/$mm^2$) and 28 (500.3 ± 61.4/$mm^2$) post-ICH (Fig. 3a, b). Ferritin, an iron storage protein, is associated with ICH-induced brain iron accumulation. The number of ferritin positive cells was also elevated at days 7 (167.9 ± 20.1/$mm^2$) and 28 (283.1 ± 21.6/$mm^2$) post-ICH compared with the Sham group (39.4 ± 6.3/$mm^2$; Fig. 3a, c). Furthermore, Western blotting revealed that the expression levels of ferritin heavy chain (FTH) and ferritin light chain (FTL) were significantly increased at days 1, 7, and 28 after ICH (Fig. 3d).

### Minocycline Prevents Post-ICH Brain Injury and Brain Iron Overload in Minipigs

To explore the optimal doses of minocycline for treating ICH, we selected four maintenance doses (1, 3, 6, and 10 mg/kg every 12 h from 12 h to 7 days after ICH) and tested the their effect by detecting the iron concentration perihematoma at day 7 and neurological scores at days 1, 7, and 28 after ICH (Figure II in the supplementary information). We found that the maintenance dose at 3 mg/kg every 12 h is the optimal dose and significantly decreased the iron content (Fig. 4(f); Figure IIa in the supplementary information) and improved neurological scores (Fig. 6c; Figure IIb in the supplementary information).

The effects of minocycline on brain edema, lesion volume, iron overload, and iron-handing proteins were evaluated after

**Fig. 1** Establishment of ICH model in minipigs and T2-weighted magnetic resonance imaging scan. **a** Images of digital stereotaxic instrument and anesthetic machine (left), ICH surgery in minipigs, and typical hematoma location at caudate nucleus (right, within red dotted lines). **b** Representative consecutive T2 images of one minipig prior to (Pre) or at days 1, 7, and 28 post-ICH (scale bar = 1 cm; red dotted area indicates brain edema, yellow dotted area reveals lateral ventricle). **c** Quantitative data of brain water content (%) for ipsilateral and contralateral brain tissue of minipigs in the Sham group or at days 1, 7, and 28 post-ICH. **d** Percentage of enlargement (%) in ipsilateral and contralateral lateral ventricles of minipigs, prior to (100%) or at days 1, 7, and 28 post-ICH. Data are shown as mean ± SD, one-way ANOVA, followed by Bonferroni post hoc test ($n = 5$ for each group; $^{*}P < 0.05$, $^{**}P < 0.01$ vs Sham group, $^{\#}P < 0.05$, $^{\#\#}P < 0.01$ vs Pre group)

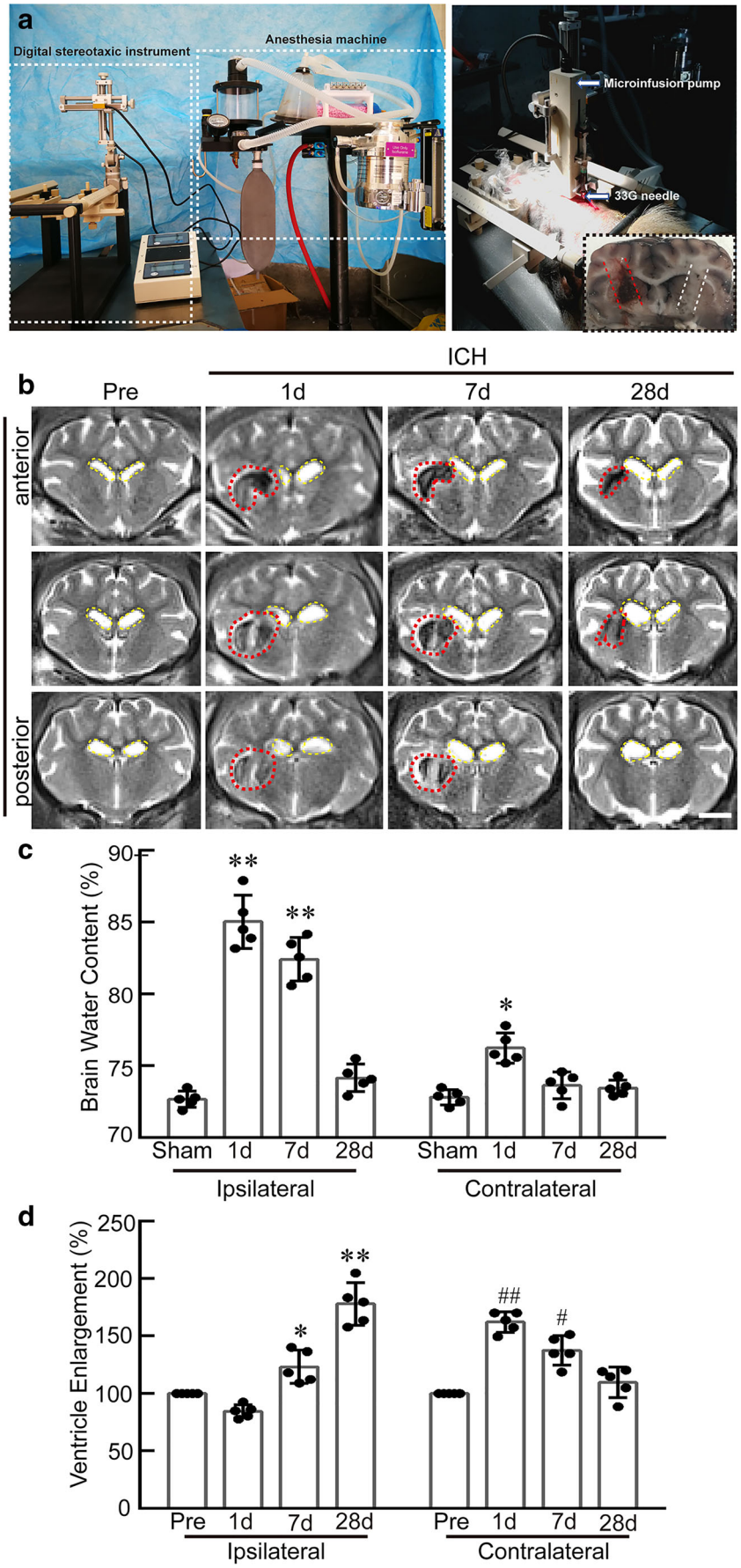
a
Digital stereotaxic instrument
Anesthesia machine
Microinfusion pump
33G needle
b
ICH
Pre
1d
7d
28d
T2
anterior
posterior
c
Brain Water Content (%)
90
85
80
75
70
**
**
*
Sham
1d
7d
28d
Sham
1d
7d
28d
Ipsilateral
Contralateral
d
Ventricle Enlargement (%)
250
200
150
100
50
0
*
**
##
#
Pre
1d
7d
28d
Pre
1d
7d
28d
Ipsilateral
Contralateral

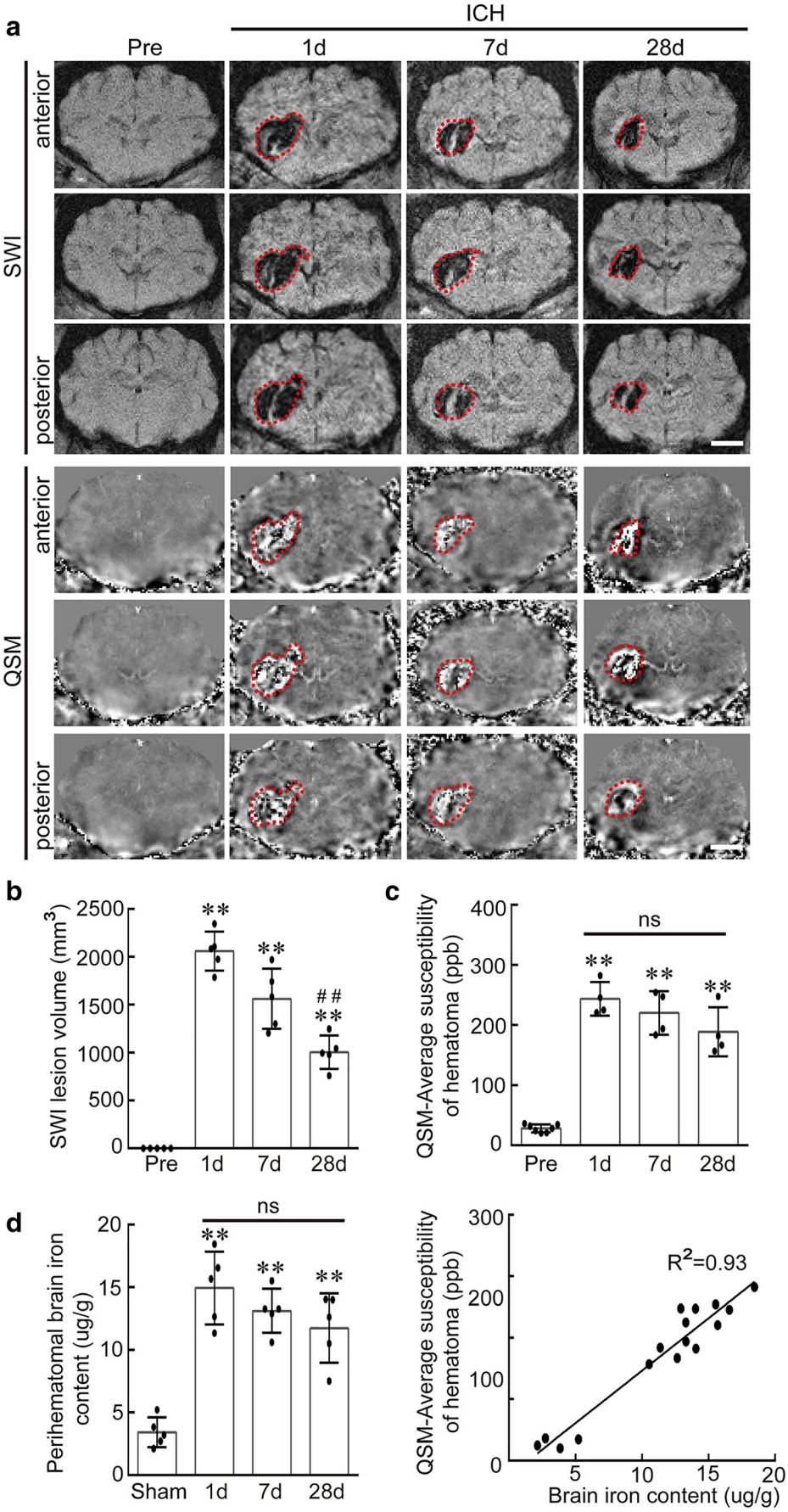
a
ICH
Pre
1d
7d
28d
SWI
anterior
posterior
QSM
anterior
posterior
b
SWI lesion volume (mm3)
2500
2000
1500
1000
500
0
**
**
##
**
Pre
1d
7d
28d
c
QSM-Average susceptibility of hematoma (ppb)
400
300
200
100
0
ns
**
**
**
Pre
1d
7d
28d
d
Perihematomal brain iron content (ug/g)
20
15
10
5
0
ns
**
**
**
Sham
1d
7d
28d
QSM-Average susceptibility of hematoma (ppb)
300
200
100
0
R2=0.93
5
10
15
20
Brain iron content (ug/g)

◀ **Fig. 2** SWI-QSM accurately and noninvasively reflects iron deposition and hematomal volume after ICH. **a** Representative SWI and QSM images of one minipig before (Pre) or at days 1, 7, and 28 after ICH (scale bar = 1 cm; red dotted area indicates hematoma region). **b** Quantitative data for volume of hematoma ($mm^3$) in minipigs prior to or post-ICH. **c** Mean susceptibility value of hematoma (ppb × $10^{-9}$) in minipigs before (Pre) or at days 1, 7, and 28 after ICH. **d** Perihematomal iron content (μg/g; left) and the linear correlation between average susceptibility and iron content (right). Data are shown as mean ± SD, one-way ANOVA, followed by Bonferroni post hoc test ($n = 4$–7 for each group; $^{**}P < 0.01$ vs Pre group; $^{\#\#}P < 0.01$ vs day 1; ns = not significant)

ICH. The value of ipsilateral brain water content was apparently decreased in minocycline group at day 7 (77.6 ± 1.4% vs 82.7 ± 1.4% in the ICH + vehicle group; $P < 0.05$; Fig. 4b, and the volume of ipsilateral ventricle was also significantly decreased after minocycline treatment at day 28 (133.8 ± 10.2% vs 186.2 ± 18.5% in the ICH + vehicle group; $P < 0.05$; Fig. 4(a, c)). In addition, the SWI lesion volume (630.3 ± 146.7 $mm^3$ vs 981.1 ± 100.7 $mm^3$ in the ICH + vehicle group; $P < 0.05$; Fig. 4(a, d)), average susceptibility (136 ± 22.7 bbp vs 198.3 ± 39.9 bbp in the ICH + vehicle group; $P < 0.05$; Fig. 4e, and perihematomal brain iron content (6.9 ± 1.1 μg/g vs 10.4 ± 1.9 μg/g in the ICH + vehicle group; $P < 0.05$; Fig. 4f were significantly reduced at day 28 following the treatment of minocycline. Furthermore, the number of perihematomal hemosiderin-positive cells was decreased at day 28 in the minocycline-treated group (278.7 ± 23.1/$mm^2$ vs 519.1 ± 46.4/$mm^2$ in the ICH + vehicle group; $P < 0.01$; Fig. 5(a, b)). Additionally, treatment of minocycline reduced the number of perihematomal ferritin-positive cells at day 28

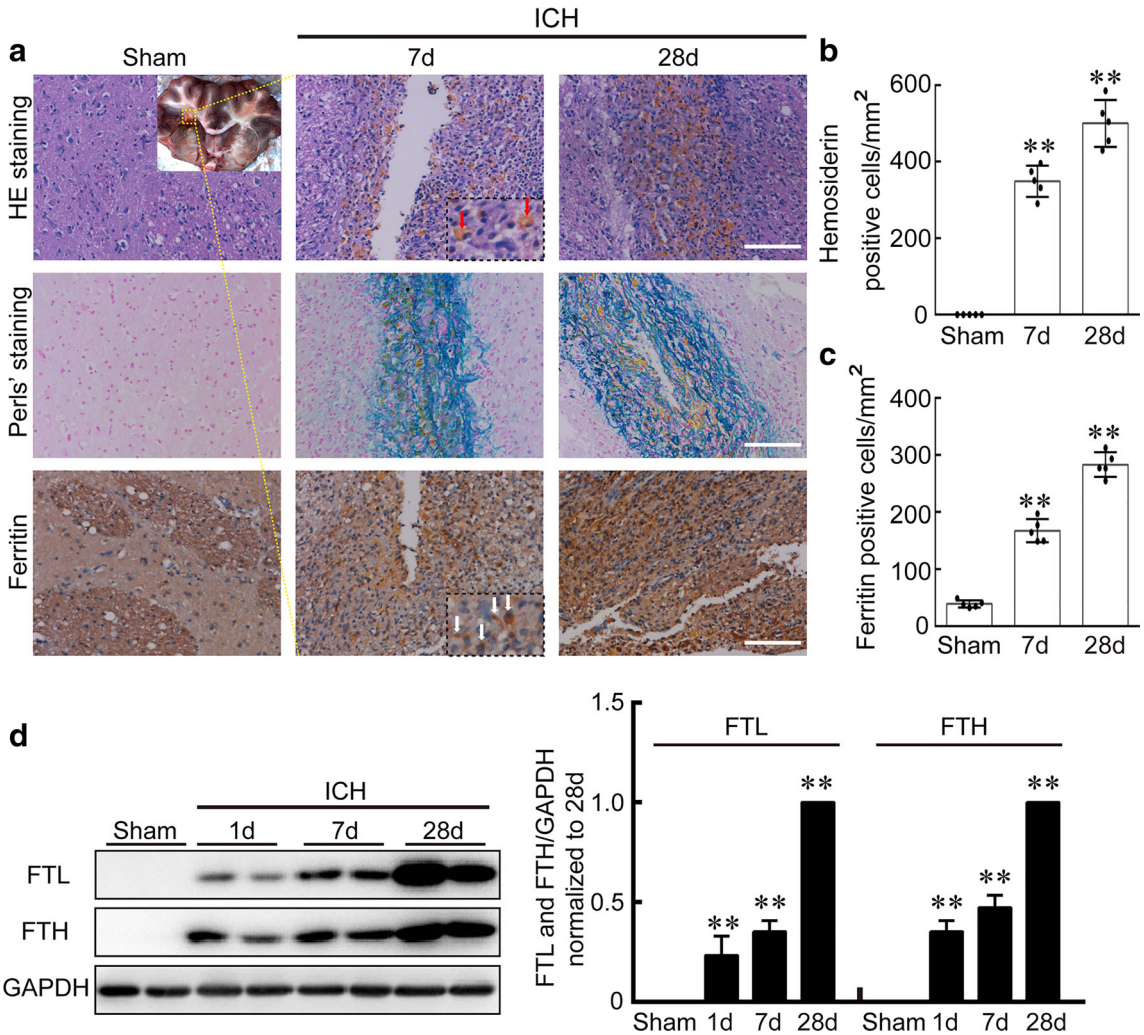


**Fig. 3** ICH leads to iron accumulation and upregulated iron handling proteins in perihematomal areas. **a** Representative HE staining indicating hemosiderin-positive cells adjacent to hematoma region (upper, typical hemosiderin-positive cells indicated by red arrows); enhanced Perls' staining revealing iron accumulation (middle); immunohistochemistry analysis of ferritin in Sham group or at days 7 and 28 post-ICH (nether, typical ferritin-positive cells indicated by white arrows, scale bar = 100 um). **b** and **c** Quantitative data of hemosiderin- and ferritin-positive cells per square millimeter in Sham and ICH group. **d** Representative Western blotting and quantitative analysis of ferritin heavy chain (FTH) and ferritin light chain (FTL) in Sham group or at days 1, 7, and 28 post-ICH. Data are shown as mean ± SD, one-way ANOVA, followed by Bonferroni post hoc test ($n = 5$ for each group; $^{**}P < 0.01$ vs Sham group)

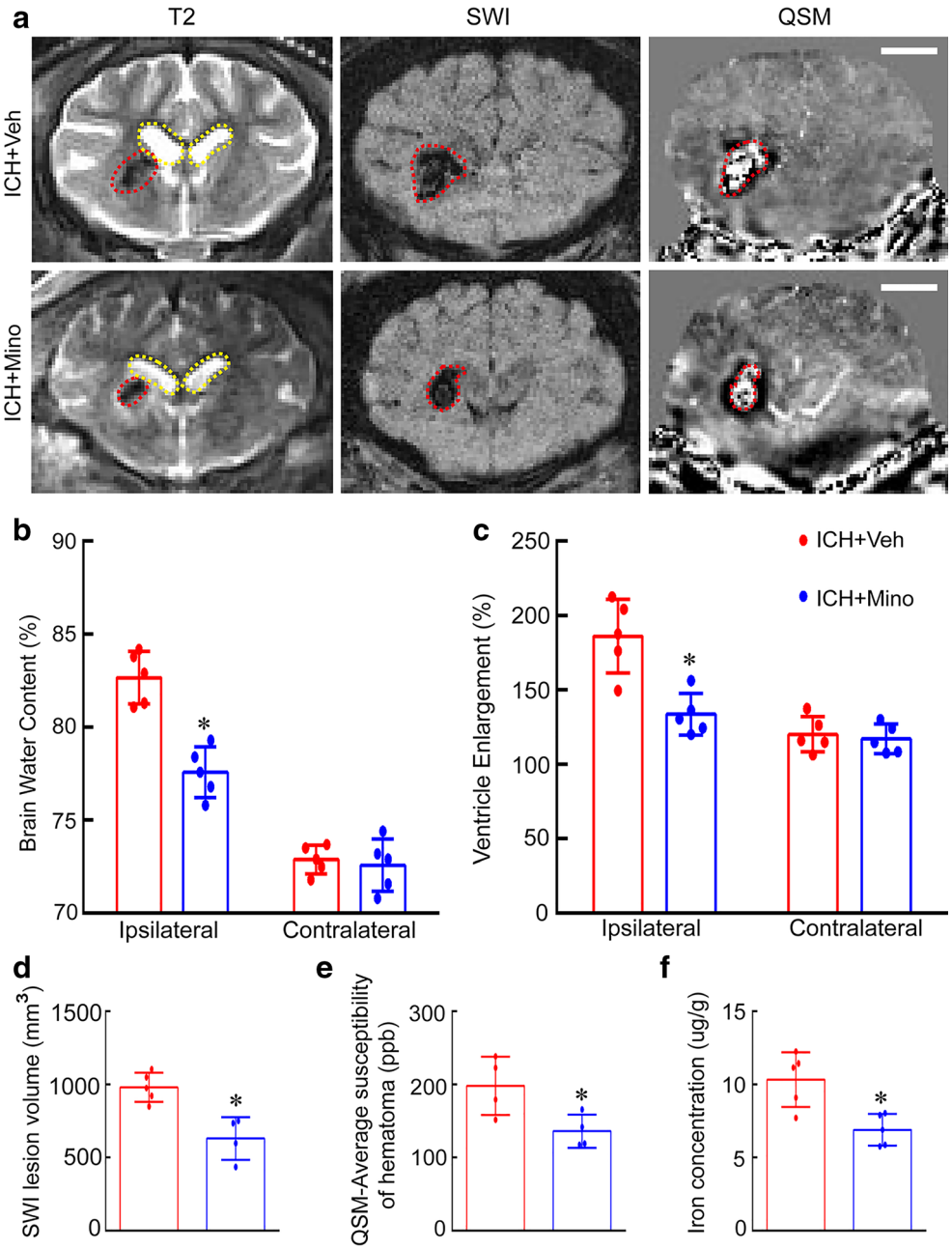


**Fig. 4** Effects of minocycline on iron content and brain injury in minipig ICH model. (a) Representative T2, SWI, and QSM images of ICH + vehicle (ICH + Veh) and ICH + minocycline (ICH + Mino) group at day 28 post-ICH (scale bar = 1 cm; red dotted area indicates hematoma region, yellow dotted area reveals lateral ventricle). (b) Quantitative data of brain water content (%) in ipsilateral and contralateral brain tissue of ICH + Veh and ICH + Mino groups at day 7 after ICH. (c) Percentage of enlargement (%) in ipsilateral and contralateral lateral ventricles of ICH + Veh and ICH + Mino groups at day 28 post-ICH (right). (d, e) Lesion volume ((d); $mm^3$) and average susceptibility ((e); ppb × $10^{-9}$) of hematoma in ICH + Veh and ICH + Mino groups at day 28 after ICH. (f) Perihematomal iron content (μg/g) in vehicle- and minocycline-treated groups. Data are shown as mean ± SD, Student's *t* test (two-tailed, unpaired) ($n = 4–5$ for each group; *$P < 0.05$ vs ICH + Veh group)

after ICH (205.3 ± 15.2/$mm^2$ vs 282.3 ± 22/$mm^2$ in the ICH + vehicle group; $P < 0.01$; Fig. 5(a–c)). The results of Western blotting also revealed that the expression levels of FTL and FTH were dramatically decreased by minocycline ($P < 0.01$; Fig. 5d.

## Minocycline Alleviates ICH-Induced White Matter Injury and Neurological Deficits in Minipigs

Notable reduction and fragmentation of nerve fiber bundles in the ipsilateral hemisphere was revealed by DTI techniques at day 28 post-ICH (Fig. 6a). In the DTI analysis, ADC reveals water diffusion within each magnetic resonance voxel, and FA indicates the fiber tract integrity and cellular structures within the fiber tracts [30]. In the ICH group, the ADC value in brain tissues adjacent to the hemorrhage was significantly increased compared with the contralateral side (2.97 ± 0.2 vs 1.41 ± 0.1 × $10^{-3}$ $mm^2$/s; $P < 0.01$), whereas the FA value was remarkably reduced (0.25 ± 0.04 vs 0.58 ± 0.06, $P < 0.01$; Fig. 6b), indicating the damage on white matter nerve fiber. However, the damage was dramatically reduced by minocycline treatment as the ADC (2.97 ± 0.2 vs 2.25 ± 0.14 × $10^{-3}$ $mm^2$/s; $P < 0.05$; Fig. 6b) and FA values (0.25 ± 0.04 vs 0.39 ± 0.04; $P < 0.05$; Fig. 6b) were brought back. Additionally, minocycline treatment also alleviated neurological deficits

at days 7 and 28 after ICH (Fig. 6c). Furthermore, treatment of minocycline also prevented axon swelling and myelin injury in white matter fiber (Fig. 6d). The number of mean axon (62.5 ± 18.9 vs 28.7 ± 8.4 per 100 μm$^2$; $P < 0.05$; Fig. 6e) was significantly increased, while the mean axon diameter (0.97 ± 0.36 vs 1.35 ± 0.56 μm; $P < 0.05$; Fig. 6e) and G-ratio (0.79 ± 0.05 vs 0.81 ± 0.06; $P < 0.05$; Fig. 6e) were decreased compared with in the ICH + vehicle group. In addition, minocycline treatment attenuated astrocyte and microglia activation compared with the control (Figure III in the supplementary information).

## Discussion

The major findings of the present study are as follows: (1) An ICH model in minipigs was established under the guidance of digital stereotactic equipment; (2) SWI-QSM was a noninvasive and accurate method for the quantification of brain iron content at acute and chronic phases after ICH; (3) Minocycline treatment could reduce the risk of post-ICH iron overload in minipigs; and (4) minocycline may attenuate ICH-induced brain edema, ventricle enlargement, lesion volume, white matter injury, and neurological deficits.

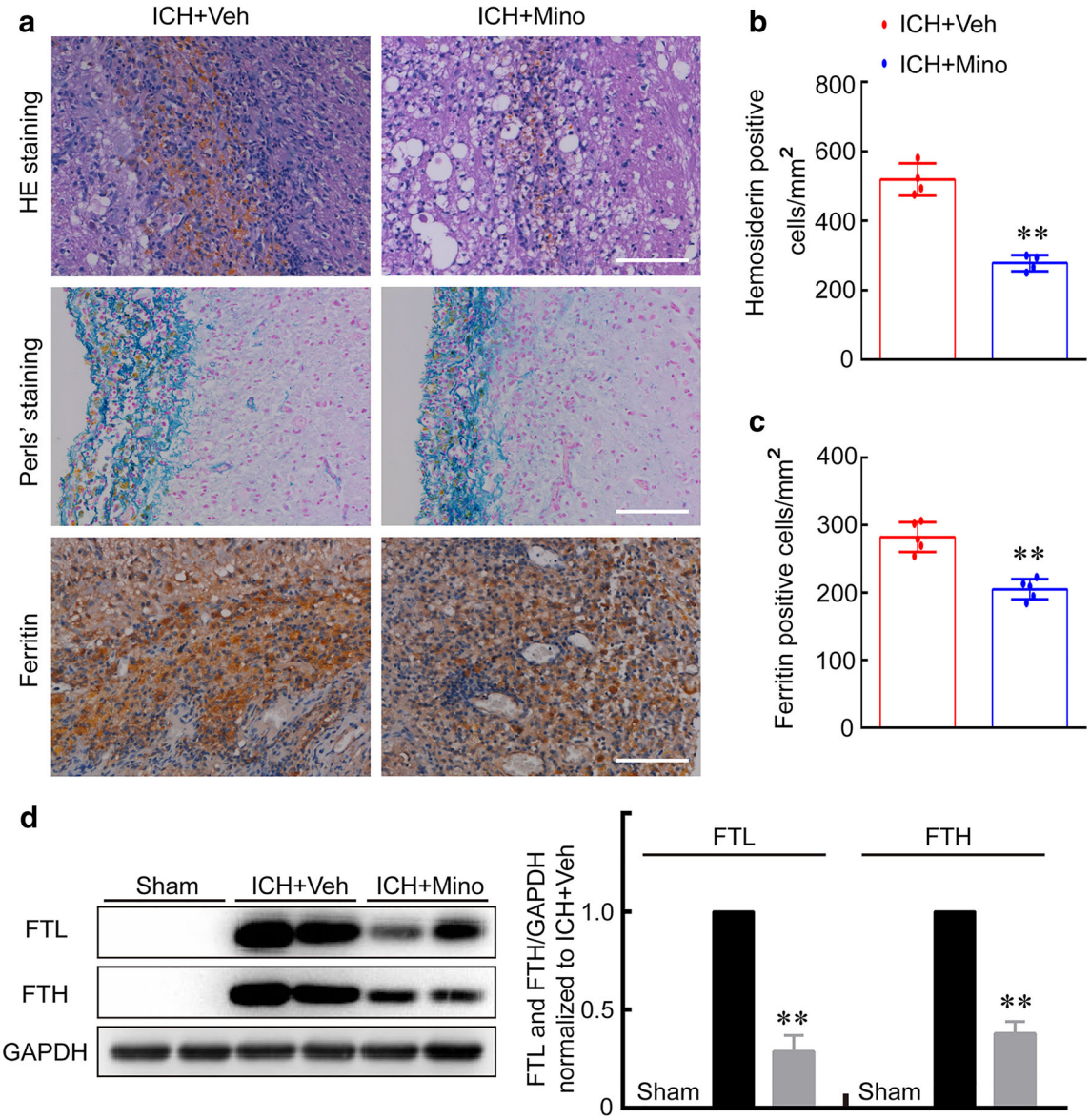


**Fig. 5** Influences of minocycline on iron accumulation and iron-handling proteins after ICH. (a) Representative images of HE staining for hemosiderin-positive cells adjacent to hematoma (upper), enhanced Perls' staining for iron accumulation (middle), and immunohistochemistry staining for ferritin (nether) in ICH + Veh and ICH + Mino groups at day 28 after ICH (scale bar = 100 um). (b and c) Quantitative data for hemosiderin- and ferritin-positive cells per square millimeter at day 28 post-ICH. (d) Western blotting and quantitative analysis of ferritin heavy chain (FTH) and ferritin light chain (FTL) in vehicle- and minocycline-treated groups. Data are shown as mean ± SD, Student's *t* test (two-tailed, unpaired) ($n = 5$ for each group; $^{**}P < 0.01$ vs ICH + Veh group)

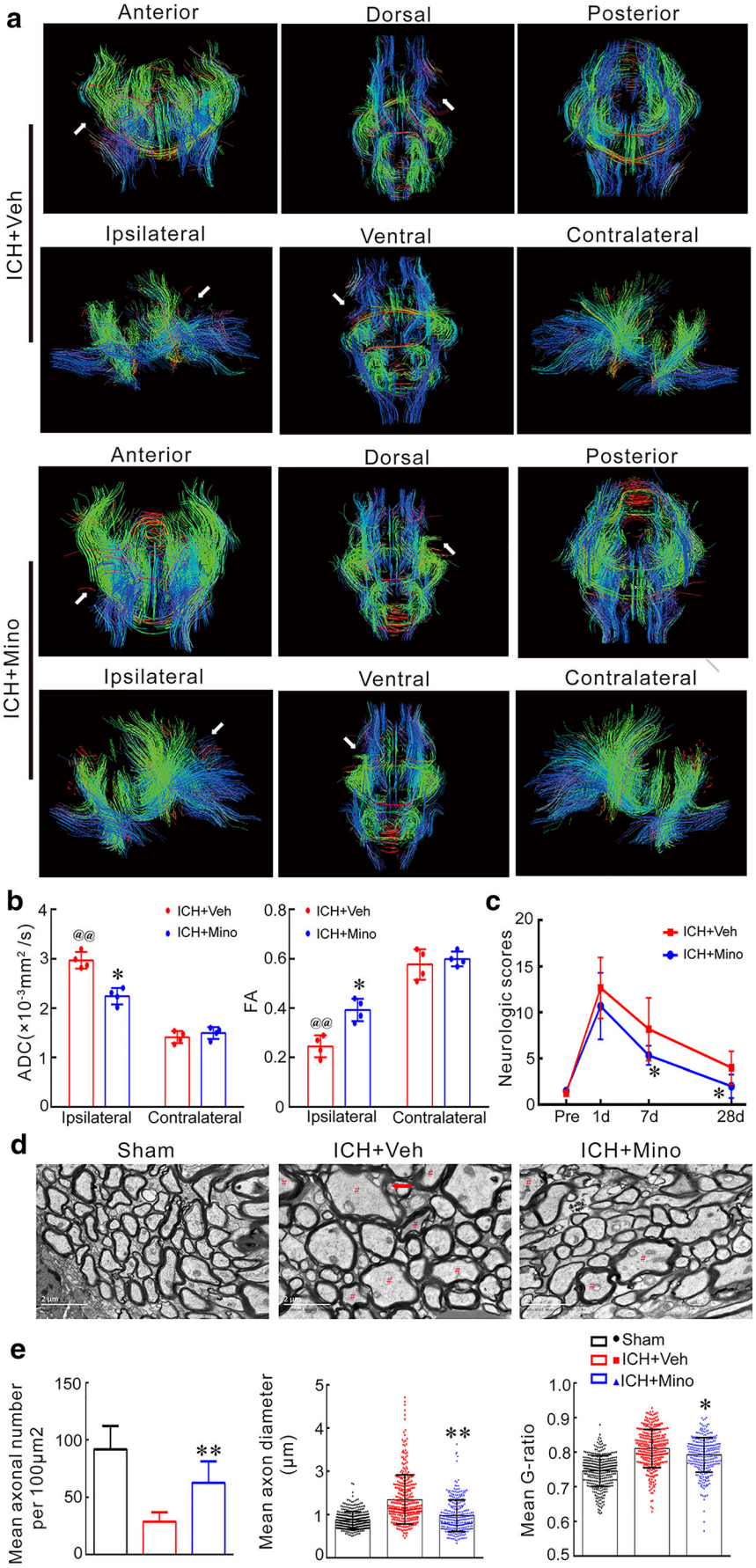
a
Anterior
Dorsal
Posterior
ICH+Veh
Ipsilateral
Ventral
Contralateral
Anterior
Dorsal
Posterior
ICH+Mino
Ipsilateral
Ventral
Contralateral
b
ADC(×10⁻³mm²/s)
ICH+Veh
ICH+Mino
@@
*
Ipsilateral
Contralateral
FA
ICH+Veh
ICH+Mino
@@
*
Ipsilateral
Contralateral
c
Neurologic scores
ICH+Veh
ICH+Mino
*
*
Pre
1d
7d
28d
d
Sham
ICH+Veh
ICH+Mino
e
Mean axonal number per 100μm2
**
Mean axon diameter (μm)
**
Sham
ICH+Veh
ICH+Mino
Mean G-ratio
*

◀ **Fig. 6** Effects of minocycline on white matter injury and neurological function in minipig ICH model. **a** Representative three-dimensional reconstruction images of white matter nerve fibers detected by DTI in ICH + Veh and ICH + Mino groups at day 28 after ICH. The hemorrhagic regions were indicated by white arrows. Anterior, dorsal, posterior, ipsilateral, ventral, and contralateral viewings were presented to reveal the white matter loss in hemorrhagic region. **b** Apparent diffusion coefficient (ADC $\times 10^{-3}$ $mm^2/s$) and fractional anisotropy (FA) of ipsilateral and contralateral areas in ICH + Veh and ICH + Mino groups at day 28 post-ICH, Student's *t* test (two-tailed, unpaired). **c** Neurological scores for ICH + Veh and ICH + Mino groups before (Pre) or at days 1, 7, and 28 after ICH, Student's t test (two-tailed, unpaired) at each timepoint. **d** Electron microscopic analysis of white matter axonal myelination adjacent to hematoma in Sham, ICH + Veh, and ICH + Mino groups (scale bar = 2 μm; number sign indicated axons with injured myelin and red arrow revealed typical injured myelin after ICH). **e** Quantitative analysis of mean axonal numbers (per 100 $\mu m^2$; left), axonal diameters (middle), and g-ratios (right) in Sham, ICH + Veh, and ICH + Mino groups at day 28 post-ICH, one-way ANOVA, followed by Bonferroni post hoc test. Data are shown as mean ± SD ($n = 4$–5 for each group; $^*P < 0.05$, $^{**}P < 0.01$ vs ICH + Veh group; $^{@@}P < 0.01$ vs contralateral side)

Experimental ICH is commonly induced in rodents; however, previous studies revealed that established models using pigs and monkeys mimic the clinical manifestations more closely in autism and Huntington model, which could not be found on rodent animal models [31, 32]. Thus, establishment of proper ICH models to mimic clinical manifestations are required for future experimental research, particularly for the preclinical studies on drug discovery. In the present study, a minipig ICH model was established under the guidance of digital stereotactic equipment and verified by morphology, behavioral tests, and quantitative neuroimaging analysis. Previous studies demonstrated that ICH-induced ventricle expansion was mainly located in the ipsilateral [3, 33], whereas our ICH pigs developed ipsilateral ventricle enlargement at 7 and 28 days and contralateral ventricle enlargement at 1 at 7 days after ICH, hematoma squeeze effect at acute stage and brain atrophy and tissue loss at chronic stage after ICH may contribute these phenomenon. What is more, post-ICH iron overload was detected, which was characterized with increased numbers of hemosiderin- and ferritin-positive cells and upregulation of perihematomal iron handling proteins. In addition, the lesion volume and brain edema were alleviated spontaneously from onset to day 28 post-ICH. These results were consistent with our previous findings in rodent ICH model [4]. Furthermore, the results of DTI and TEM analysis revealed the white matter injury induced by ICH. These data indicated that our minipig ICH model was stable and could mimic the pathology of ICH.

Iron is an essential element associated with numerous biological functions, including oxygen and electron transport, redox reactions, cell division, nucleotide synthesis, and myelination [34]. In the brain, iron homeostasis is crucial; however, a variety of degenerative neurological and psychiatric disorders could result in excessive iron accumulation in brain, such as Alzheimer's disease, Huntington's Chorea, multiple sclerosis, and Parkinson's disease [35–37]. Furthermore, brain iron overload induced by experimental ICH could lead to perihematomal brain edema, neuronal death, brain atrophy, and neurological deficits [38]. Thus, quantification of iron concentration in vivo is necessary, which could help to understand the regulatory functions of iron in the pathogenesis of ICH or other diseases. Previous study revealed that the R2* mapping was a promising approach on the evaluation of post-ICH brain iron overload; however, the MRI R2* mapping could not be used to determine the iron levels in hematoma at acute phase (too high) or in the cavity at chronic phase after ICH [9]. Therefore, the QSM method based on susceptibility-weighted images was a more promising method to estimate the tissue iron content following ICH.

Although one previous clinical study had shown that the QSM signal changed significantly from days 2 to 30 after ICH, it only reported one case [16]. Our QSM results in minipigs revealed that average susceptibility and iron content of hematoma decreased spontaneously from onset to day 28 post-ICH as previous results [4, 12, 16, 18], but not significant. Similarly, although clinical study has indicated that inflammation and brain edema could be alleviated spontaneously within 1 month following ICH, the motor function is still limited with little improvement within 1 month, and 2/3 of the patients are moderately or severely disabled [39, 40], indicating that persistent iron overload might contribute limited functional recovery after ICH. What is more, the course of motor recovery could be determined by the integrity of the white matter as measured by DTI [41]. DTI was used in the present study to map white matter tractography adjacent to hematoma in minipig ICH model; increased ADC values and reduced FA values were detected in the ICH group, indicating the dysfunction of white matter fiber. What is more, the results of TEM revealed reduced axon number and axonal swelling in the ICH group, accompanied by motor impairment. These results reveled that white matter might be vulnerable to iron toxicity; long-term iron overload might lead to persistent white matter injury and irrecoverable post-ICH motor dysfunction. Thus, iron-targeted therapy is a promising method to ICH, which needs more experimental and clinical works to explore.

In addition, average susceptibility could be an accurate and noninvasive assessment to reflect the perihematomal iron concentration, and the average susceptibility and iron content were positively correlated ($R^2 = 0.93$). In view of the close relationship between iron deposition and ICH development and prognosis [3, 34, 38], SWI-QSM could be used in the prognosis judgment and evaluation of treatment effect related to iron in clinical and basic research in the future, which should receive more attention and promotion.

Previous studies have suggested that minocycline is a potential iron chelator and an inhibitor of microglial activation, and it can prevent ICH-induced brain iron overload and brain injury in rodent animal ICH model [9, 19]. In clinical research, although several retrospective cohort studies revealed that treatment with minocycline was associated with improved outcome following acute ICH, no large prospective randomized trials have been conducted so far [21]. Recently, an early-phase randomized trial including 16 eligible patients indicated that oral administration of minocycline was safe, but exhibited no effects on hematoma volume and perihematomal edema [42]. Thus, more preclinical studies are required to investigate the effects of minocycline on ICH patients, and the dosage and duration need to be optimized using rodent animal model and/or large gyrencephalic species. In the present study, the influences of minocycline were evaluated using the minipig ICH model. After screening the dosage, we found that a maintenance dose of 3 mg/kg every 12 h for up to 7 days was the optimum; this dose of minocycline could prevent ICH-induced brain injury in minipigs by reducing iron deposition, brain edema, and white matter injury in the perihematomal region. As an inhibitor of microglial activation, minocycline also reduced the number of Iba-1-positive microglia. Interestingly, minocycline treatment decreased GFAP-positive astrocytes, which could be due to the inhibition of microglia [43]. Furthermore, DTI results indicated that minocycline treatment could alleviate white matter injury by reducing ADC values and axon swelling and increasing FA values and axonal density. What is more, there are still some further works for us following this paper. For example, the impact of sex on neurological disease has been gaining more and more attention in both clinical and preclinical research, we will use both male and female minipigs to explore more promising drugs for ICH treatment.

## Conclusion

The present study demonstrated that the QSM is a noninvasive and reliable method for the assessment of iron overload and iron-mediated treatments in cerebral hemorrhage at acute and chronic phases. Systemic administration of minocycline could reduce ICH-induced brain iron overload, brain edema, and white matter injury in the minipig ICH model.

**Authors' Contributions** Y.Y., K.Z., and T.C. designed the experiments. X.Y. scanned and analyzed all MRI images. X.L., X.C., J.W., Y.Q., L.Y., Z.J., Q.C., J.X., Y.L., and Q.H. preformed the experiments and discussed the results. X.Z. collected and analyzed all the present data. Y.Y., H.F., and T.C. wrote the draft and worked on the manuscript revision. All authors read and approved the final manuscript.

**Funding Information** The present study was funded by Southwest Hospital (grant no. SWH2017JSZD-10 and SWH2016ZDCX1011) and the National Basic Research Program of China (973 Program, no. 2014CB541600).

## Compliance with Ethical Standards

All experiments are reported in compliance with the Animal Research: Reporting in Vivo Experiments (ARRIVE) guidelines. The experimental protocols were approved by the Ethics Committee of the Third Military Medical University and performed according to the guide for the care and use of laboratory animals. All institutional and national guidelines for the care and use of laboratory animals were followed.

**Conflict of Interest** The authors declare that they have no conflict of interest.

## References

1. Cordonnier C, Demchuk A, Ziai W, Anderson CS. Intracerebral haemorrhage: current approaches to acute management. Lancet (London, England). 2018;392(10154):1257–68. https://doi.org/10.1016/s0140-6736(18)31878-6.
2. Xi G, Keep RF, Hoff JT. Mechanisms of brain injury after intracerebral haemorrhage. Lancet Neurol. 2006;5(1):53–63. https://doi.org/10.1016/s1474-4422(05)70283-0.
3. Hua Y, Nakamura T, Keep RF, Wu J, Schallert T, Hoff JT, et al. Long-term effects of experimental intracerebral hemorrhage: the role of iron. J Neurosurg. 2006;104(2):305–12. https://doi.org/10.3171/jns.2006.104.2.305.
4. Chen Q, Tang J, Tan L, Guo J, Tao Y, Li L, et al. Intracerebral hematoma contributes to hydrocephalus after intraventricular hemorrhage via aggravating Iron accumulation. Stroke. 2015;46(10):2902–8. https://doi.org/10.1161/strokeaha.115.009713.
5. Xie Q, Gu Y, Hua Y, Liu W, Keep RF, Xi G. Deferoxamine attenuates white matter injury in a piglet intracerebral hemorrhage model. Stroke. 2014;45(1):290–2. https://doi.org/10.1161/strokeaha.113.003033.
6. Zhao F, Hua Y, He Y, Keep RF, Xi G. Minocycline-induced attenuation of iron overload and brain injury after experimental intracerebral hemorrhage. Stroke. 2011;42(12):3587–93. https://doi.org/10.1161/strokeaha.111.623926.
7. Gu Y, Hua Y, Keep RF, Morgenstern LB, Xi G. Deferoxamine reduces intracerebral hematoma-induced iron accumulation and neuronal death in piglets. Stroke. 2009;40(6):2241–3. https://doi.org/10.1161/strokeaha.108.539536.
8. Yu Y, Zhao W, Zhu C, Kong Z, Xu Y, Liu G, et al. The clinical effect of deferoxamine mesylate on edema after intracerebral hemorrhage. PLoS One. 2015;10(4):e0122371. https://doi.org/10.1371/journal.pone.0122371.
9. Cao S, Hua Y, Keep RF, Chaudhary N, Xi G. Minocycline effects on intracerebral hemorrhage-induced iron overload in aged rats: brain Iron quantification with magnetic resonance imaging. Stroke. 2018;49(4):995–1002. https://doi.org/10.1161/strokeaha.117.019860.
10. Wood JC, Enriquez C, Ghugre N, Tyzka JM, Carson S, Nelson MD, et al. MRI R2 and R2* mapping accurately estimates hepatic iron

concentration in transfusion-dependent thalassemia and sickle cell disease patients. Blood. 2005;106(4):1460–5. https://doi.org/10.1182/blood-2004-10-3982.
11. Yokoo T, Yuan Q, Senegas J, Wiethoff AJ, Pedrosa I. Quantitative R2* MRI of the liver with rician noise models for evaluation of hepatic iron overload: simulation, phantom, and early clinical experience. J Magn Reson Imaging. 2015;42(6):1544–59. https://doi.org/10.1002/jmri.24948.
12. Chang S, Zhang J, Liu T, Tsiouris AJ, Shou J, Nguyen T, et al. Quantitative susceptibility mapping of intracerebral hemorrhages at various stages. J Magn Reson Imaging. 2016;44(2):420–5. https://doi.org/10.1002/jmri.25143.
13. Cronin MJ, Wang N, Decker KS, Wei H, Zhu WZ, Liu C. Exploring the origins of echo-time-dependent quantitative susceptibility mapping (QSM) measurements in healthy tissue and cerebral microbleeds. NeuroImage. 2017;149:98–113. https://doi.org/10.1016/j.neuroimage.2017.01.053.
14. Wycliffe ND, Choe J, Holshouser B, Oyoyo UE, Haacke EM, Kido DK. Reliability in detection of hemorrhage in acute stroke by a new three-dimensional gradient recalled echo susceptibility-weighted imaging technique compared to computed tomography: a retrospective study. J Magn Reson Imaging. 2004;20(3):372–7. https://doi.org/10.1002/jmri.20130.
15. Haque ME, Gabr RE, Zhao X, Hasan KM, Valenzuela A, Narayana PA, et al. Serial quantitative neuroimaging of iron in the intracerebral hemorrhage pig model. J Cereb Blood Flow Metab. 2018;38(3):375–81. https://doi.org/10.1177/0271678x17751548.
16. Sun H, Klahr AC, Kate M, Gioia LC, Emery DJ, Butcher KS, et al. Quantitative susceptibility mapping for following intracranial hemorrhage. Radiology. 2018;288(3):830–9. https://doi.org/10.1148/radiol.2018171918.
17. Vaas M, Deistung A, Reichenbach JR, Keller A, Kipar A, Klohs J. Vascular and tissue changes of magnetic susceptibility in the mouse brain after transient cerebral ischemia. Transl Stroke Res. 2018;9(4):426–35. https://doi.org/10.1007/s12975-017-0591-x.
18. Dai S, Hua Y, Keep RF, Novakovic N, Fei Z, Xi G. Minocycline attenuates brain injury and iron overload after intracerebral hemorrhage in aged female rats. Neurobiol Dis. 2018;126:76–84. https://doi.org/10.1016/j.nbd.2018.06.001.
19. Tang J, Chen Q, Guo J, Yang L, Tao Y, Li L, et al. Minocycline attenuates neonatal germinal-matrix-hemorrhage-induced neuroinflammation and brain edema by activating cannabinoid receptor 2. Mol Neurobiol. 2016;53(3):1935–48. https://doi.org/10.1007/s12035-015-9154-x.
20. Chen-Roetling J, Chen L, Regan RF. Minocycline attenuates iron neurotoxicity in cortical cell cultures. Biochem Biophys Res Commun. 2009;386(2):322–6. https://doi.org/10.1016/j.bbrc.2009.06.026.
21. Malhotra K, Chang JJ, Khunger A, Blacker D, Switzer JA, Goyal N, et al. Minocycline for acute stroke treatment: a systematic review and meta-analysis of randomized clinical trials. J Neurol. 2018;265(8):1871–9. https://doi.org/10.1007/s00415-018-8935-3.
22. Yang Q, Zhou L, Liu C, Liu D, Zhang Y, Li C, et al. Brain iron deposition in type 2 diabetes mellitus with and without mild cognitive impairment-an in vivo susceptibility mapping study. Brain Imaging Behav. 2018;12:1479–87. https://doi.org/10.1007/s11682-017-9815-7.
23. Bilgic B, Pfefferbaum A, Rohlfing T, Sullivan EV, Adalsteinsson E. MRI estimates of brain iron concentration in normal aging using quantitative susceptibility mapping. NeuroImage. 2012;59(3):2625–35. https://doi.org/10.1016/j.neuroimage.2011.08.077.
24. Haacke EM, Tang J, Neelavalli J, Cheng YC. Susceptibility mapping as a means to visualize veins and quantify oxygen saturation. J Magn Reson Imaging. 2010;32(3):663–76. https://doi.org/10.1002/jmri.22276.
25. Du H, Xie B, Lu P, Feng H, Wang J, Yuan S. Impaired white-matter integrity in photosensitive epilepsy: a DTI study using tract-based spatial statistics. J Neuroradiol. 2014;41(2):131–5. https://doi.org/10.1016/j.neurad.2013.06.002.
26. Yang F, Wang Z, Zhang JH, Tang J, Liu X, Tan L, et al. Receptor for advanced glycation end-product antagonist reduces blood-brain barrier damage after intracerebral hemorrhage. Stroke. 2015;46(5):1328–36. https://doi.org/10.1161/strokeaha.114.008336.
27. Yang Y, Zhang X, Ge H, Liu W, Sun E, Ma Y, et al. Epothilone B benefits nigrostriatal pathway recovery by promoting microtubule stabilization after intracerebral hemorrhage. J Am Heart Assoc. 2018;7(2). https://doi.org/10.1161/jaha.117.007626.
28. Yang Y, Zhang K, Zhong J, Wang J, Yu Z, Lei X, et al. Stably maintained microtubules protect dopamine neurons and alleviate depression-like behavior after intracerebral hemorrhage. Sci Rep. 2018;8(1):12647. https://doi.org/10.1038/s41598-018-31056-7.
29. Tanaka Y, Imai H, Konno K, Miyagishima T, Kubota C, Puentes S, et al. Experimental model of lacunar infarction in the gyrencephalic brain of the miniature pig: neurological assessment and histological, immunohistochemical, and physiological evaluation of dynamic corticospinal tract deformation. Stroke. 2008;39(1):205–12. https://doi.org/10.1161/strokeaha.107.489906.
30. Tsougos I, Bakosis M, Tsivaka D, Athanassiou E, Fezoulidis I, Arvanitis D, et al. Diagnostic performance of quantitative diffusion tensor imaging for the differentiation of breast lesions at 3T MRI. Clin Imaging. 2019;53:25–31. https://doi.org/10.1016/j.clinimag.2018.10.002.
31. Yan S, Tu Z, Liu Z, Fan N, Yang H, Yang S, et al. A huntingtin knockin pig model recapitulates features of selective neurodegeneration in Huntington's disease. Cell. 2018;173(4):989–1002 e13. https://doi.org/10.1016/j.cell.2018.03.005.
32. Liu Z, Li X, Zhang JT, Cai YJ, Cheng TL, Cheng C, et al. Autism-like behaviours and germline transmission in transgenic monkeys overexpressing MeCP2. Nature. 2016;530(7588):98–102. https://doi.org/10.1038/nature16533.
33. MacLellan CL, Silasi G, Poon CC, Edmundson CL, Buist R, Peeling J, et al. Intracerebral hemorrhage models in rat: comparing collagenase to blood infusion. J Cereb Blood Flow Metab. 2008;28(3):516–25. https://doi.org/10.1038/sj.jcbfm.9600548.
34. Kuhn LC. Iron regulatory proteins and their role in controlling iron metabolism. Metallomics. 2015;7(2):232–43. https://doi.org/10.1039/c4mt00164h.
35. Zecca L, Berg D, Arzberger T, Ruprecht P, Rausch WD, Musicco M, et al. In vivo detection of iron and neuromelanin by transcranial sonography: a new approach for early detection of substantia nigra damage. Mov Disord. 2005;20(10):1278–85. https://doi.org/10.1002/mds.20550.
36. Quintana C, Bellefqih S, Laval JY, Guerquin-Kern JL, Wu TD, Avila J, et al. Study of the localization of iron, ferritin, and hemosiderin in Alzheimer's disease hippocampus by analytical microscopy at the subcellular level. J Struct Biol. 2006;153(1):42–54. https://doi.org/10.1016/j.jsb.2005.11.001.
37. Swaiman KF. Hallervorden-Spatz syndrome and brain iron metabolism. Arch Neurol. 1991;48(12):1285–93.
38. Garton T, Keep RF, Hua Y, Xi G. Brain iron overload following intracranial haemorrhage. Stroke Vasc Neurol. 2016;1(4):172–84. https://doi.org/10.1136/svn-2016-000042.
39. Kitago T, Ratan RR. Rehabilitation following hemorrhagic stroke: building the case for stroke-subtype specific recovery therapies.

F1000Research. 2017;6:2044. https://doi.org/10.12688/f1000research.11913.1.
40. Balami JS, Buchan AM. Complications of intracerebral haemorrhage. Lancet Neurol. 2012;11(1):101–18. https://doi.org/10.1016/s1474-4422(11)70264-2.
41. Lee KB, Kim JS, Hong BY, Kim YD, Hwang BY, Lim SH. The motor recovery related with brain lesion in patients with intracranial hemorrhage. Behav Neurol. 2015;2015:258161. https://doi.org/10.1155/2015/258161.
42. Fouda AY, Newsome AS, Spellicy S, Waller JL, Zhi W, Hess DC, et al. Minocycline in acute cerebral hemorrhage: an early phase randomized trial. Stroke. 2017;48(10):2885–7. https://doi.org/10.1161/strokeaha.117.018658.
43. Liddelow SA, Guttenplan KA, Clarke LE, Bennett FC, Bohlen CJ, Schirmer L, et al. Neurotoxic reactive astrocytes are induced by activated microglia. Nature. 2017;541(7638):481–7. https://doi.org/10.1038/nature21029.